Korean J. Chem. Eng., 34(2), 511-522 (2017)
DOI: 10.1007/s11814-016-0293-1

pISSN: 0256-1115
eISSN: 1975-7220

Heterogeneous photocatalytic degradation of phenol and derivatives by ($BiPO_4/H_2O_2/UV$ and $TiO_2/H_2O_2/UV$) and the evaluation of plant seed toxicity tests

Léa Elias Mendes Carneiro Zaidan*,†, Joan Manuel Rodriguez-Díaz, Daniella Carla Napoleão*, Maria da Conceição Branco da Silva de Mendonça Montenegro***, Alberto da Nova Araújo***, Mohand Benachour*, and Valdinete Lins da Silva***

*Chemical Engineering Department, Federal University of Pernambuco,
Avenida Prof. Artur de Sá, s/n, 50740-521 Recife, Brazil
**Instituto de Investigación, Universidad Técnica de Manabí, Av. Urbina y Che Guevara, Portoviejo, Manabí, Ecuador
***Pharmacy Factory, REQUIMTE/Department of Chemical Sciences, University Porto,
Rua Jorge Viterbo Ferreira, 228, Porto, 4050-313, Portugal
(*Received 26 July 2016 • accepted 15 October 2016*)

Abstract−We examined the photocatalytic degradation of phenol from laboratory samples under UV radiation by using $BiPO_4/H_2O_2$ and TiO_2/H_2O_2 advanced oxidation systems. Both catalysts prepared were characterized by scanning electron microscopy, Fourier transform infrared and X-ray diffraction. Surface area tests showed about 3.46 and 31.33 $m^2 \cdot g^{-1}$, respectively, for $BiPO_4$ and TiO_2. A central composite design was developed with the following variables--catalyst concentration, time and concentration of hydrogen peroxide--to optimize the degradation process. Removal rates of 99.99% for phenol degradation using $BiPO_4$ and TiO_2 were obtained, respectively. For mineralization of organic carbon were obtained 95,56% when using $BiPO_4$ and 63,40% for TiO_2, respectively. The lumped kinetic model represented satisfactorily the degradation of phenol process, using $BiPO_4/H_2O_2/UV$ (R^2=0.9977) and $TiO_2/H_2O_2/UV$ (R^2=0.9701) treatments. The toxicity tests using different seed species showed the benefits of the proposed advanced oxidation process when applied to waste waters containing these pollutants.

Keywords: Phenol, Effluents, Heterogeneous Photocatalysis, Reactor

INTRODUCTION

The demand for oil is predicted to rise to approximately 107 million barrels per day in the next decade (mbpd), representing around 32% of the world energetic supply by 2030. Given these perspectives, the industrial reserves are expected to globally contribute to the increase in environmental pollution [4-6].

The petroleum industry effluents contain a series of pollutants that vary both in composition and concentrations harmful to the environment, especially to living organisms [7,8]. Within the common pollutants found, the phenolic compounds can be highlighted due to their high bioaccumulation and toxicity, of carcinogenic and mutagenic effects [9-13].

The conventional biological degradation processes used in the treatment of effluents containing these pollutants are not sufficiently effective in the degradation of these types of compounds, due to low biodegradability; with the application of alternative techniques being strictly necessary for the complete degradation of these products [14-17]. Among these, advanced oxidation processes (AOP) are seen as beneficial, given that they provide the degradation of organic compounds, resulting in the reduction or even total mineralization of the toxic organic compounds present in wastewater [18-20]. Considering the different types of AOP available, heterogeneous photocatalysis is considered an interesting alternative, as the use of a catalyst leads to a decrease in temperature and pressure, improving the degradation rates and resulting in a more economical process [21,22].

Different types of catalysts are used in the AOP. However, according to Avisar et al. [23] and Barakat et al. [24], the use of titanium dioxide (TiO_2) as a catalyst is regarded as more advantageous, due to its low cost, non-toxicity, insolubility in water, and especially because of its chemical stability and photo-stability over a high range of pH values, being possible to be activated with sunlight. Beside this, the TiO_2 can also be used in its natural form or synthesized in combination with a variety of other metal oxides, which contribute in increasing its catalytic activity [25]. According to some studies, it was used in photocatalytic reactors in its suspended form [26] or coated on glass spheres or nanotubes [27].

Another type of composite mentioned is bismuth phosphate ($BiPO_4$), a semi-conductor that can be activated by visible radiation and has potential applications in detecting ions, separating radioactive elements, as well as in catalysis. However, it has been rarely referenced as a catalyst for environmental remediation. Yet, a recent work proposed by Bothwell et al. [28] and Liu et al. [29] demonstrated its excellent photocatalytic activity in the presence of hydrogen peroxide (H_2O_2), promoting significant improvement in the degradation of organic compounds such as methylene blue, methyl orange, rhodamine B and carbamazepine, with degrada-

†To whom correspondence should be addressed.
E-mail: leazaidan@yahoo.com.br

tion rates of about 100% [30,31].

Although both compounds mentioned are considered excellent catalysts for the degradation of organic compounds, the $BiPO_4$ has been reported in the literature as also being used in the degradation of phenolic compounds. Thus, this work is aimed at exploring the efficiency of TiO_2 and $BiPO_4$ as catalysts under UV radiation for phenolic compounds as monitoring pollutants in the degradation by HPLC-UV detection and the mineralization by Total Organic Carbon (TOC) analysis. To optimize the efficiency of the process, a statistical technique (response surface methodology) was followed, enabling us to predict the effect of each individual experimental parameter over the extension of degradation and mineralization. To evaluate the risks caused by intermediate products resulting from the oxidation process of acute toxicity studies, different types of seeds were also used to expose them before and after the process to photocatalytic treatment.

EXPERIMENTAL

1. Reagents and Standards

TiO_2 was obtained from Degussa P25, and for the preparation of $BiPO_4$, chemical products such as $Bi(NO_3)_3{\cdot}5H_2O$ and $Na_3PO_4{\cdot}12H_2O$ were attained from Sigma Aldrich Inc. Phenol (C_6H_6O), Resorcinol ($C_6H_6O_2$), Catechol ($C_6H_6O_2$), Hydroquinone ($C_6H_4(OH)_2$), p-benzoquinone ($C_6H_4O_2$) and Fumaric ($C_4H_4O_4$), Malonic($C_3H_4O_4$), Maleic ($C_4H_4O_4$) and Succinic ($C_4H_6O_4$) acids were obtained from Chem Service Inc. (purity ≥99.5%). For High-performance liquid chromatography (HPLC), the chemical products used for the preparation of the mobile phase include Milli-Q Ultrapure water, orthophosphoric acid (H_3PO_4, 85-88%, Merck) and Methanol (CH_3OH, Merck). The aqueous phenol solutions used as standard solution were prepared with distilled water.

2. Catalyst Preparation and Characterization

The TiO_2 used as a catalyst was commercially available (P25, about 70% anatase and 30% rutilum) and was obtained from Degussa Inc. $BiPO_4$ was synthesized by using a hydrothermal process, adding 3 mMole of $Bi(NO_3)_3{\cdot}5H_2O$ and 120 mL of distilled water into a recipient under magnetic stirring. A volume corresponding to 10.8 mMol of $NaH_2PO_4{\cdot}2H_2O$ was added to the previous mixture and stirred for one hour. The resulting suspension was transferred to a Teflon-lined stainless steel autoclave and kept at 160 °C for 24 hours. The solid product obtained was washed threefold with distilled water and dried at 120 °C for 12 hours.

Both catalysts (the TiO_2 and the $BiPO_4$) went through X-ray fluorescence analysis for chemical characterization. For this purpose, a Rigaku® Spectrometer RIX 300 (Japan), equipped with an Rh tube was used. The catalyst surface areas were determined by BET technique, 2.375 Micromeritics Analytical Surface Area (USA), at a pressure of 0.02 Mpa·mins^{-1} and a settling time of 30 seconds. The X-ray diffraction analysis used an X'PERT Philips Instrument (Almelo, the Netherlands), with Cupper Kα radiation, at 40 KV, 40 mA, wavelength of 1.542 Å and slit size of 0.02 2Θ. The scanning electron microscopy analysis, together with the energy-dispersive X-ray spectroscopy, was run in gold-coated cathodic pulverization of SBA samples. The microscopy was made using an electronic LEO 440i scanning microscope (Cambridge, UK) attached to a 7060 Oxford system of Energy-dispersive X-ray (EDX), enabling the chemical composition qualitative determination.

3. Configuration of the Reactor for Phenol Degradation

The phenol degradation process was applied to a photochemical annular reactor, consisting of an exterior Pyrex® glass along the longitudinal axis, made of quartz glass tube. The reactor with a capacity of 0.7 L was attached to an external recirculation tank of 1.6 L. The total volume of the solution to be treated was 2.3 L, with a flow of 1.95 L·min^{-1}. As a UV-generator, a mercury-vapor light (Philips HPLN) with an average pressure and power of 80 W was used. The system temperature during the reaction was kept between 20 °C and 25 °C by using a thermostatic bath attached to the reactor; the hydrogen peroxide solution was continuously added to the reactor using a PROVITEC PM-5900 model peristaltic pump, at a flow rate of 1.75 mL·min^{-1}. The HPLC and TOC analyses were run in samples collected periodically from the reactor after its filtration in filters with 0.22 mm pores (Millipore).

4. Trial Design and Statistical Analysis

Response surface methodology (RSM) and statistical analysis were used with the results to create optimal phenol degradation and mineralization conditions, applying $BiPO_4/H_2O_2$/UV and TiO_2/H_2O_2/UV treatment systems, respectively. Central composite design (CCD) was used, with an expansion of the points used (+1.68 and −1.68), including six trial conditions and the center axial point being obtained after three repetitions, with a total of 17 experiments. The following variables were studied: catalyst concentration, H_2O_2 concentration and reaction time. The results were analyzed statistically using the Statistics Package for Windows®, version 6.0 Statsoft.

5. The Kinetics of Mineralization of Phenol and its Derivatives

The photocatalytic kinetics of phenol and its derivatives was made by using the mineralization study of the compounds and its determination by TOC analysis. The forecasting evolution of the concentration of initial compounds during the optimised conditions of AOP was based on the *Lumped Kinetic Model* (*LKM*) [32], describing the residual total organic carbon profile (TOC/TOC_0) in the liquid phase over reaction time. Fig. 1 describes the kinetic behaviour of the catalytic oxidation of organic compounds.

Here (A) represents the group consisting of non-refractory carbon derivatives, which can be directly degraded in CO_2 and H_2O (C) or can form derivatives a carbon of the refractory group (B), and its intermediates can be converted in CO_2 and H_2O. k_1, k_2 and k_3 are the respective constant rates for each of the reactions.

6. Analytical Methods

The identification and quantification of phenol and its derivatives involved using an HPLC Shimadzu Equipment, model SS-550, equipped with a reversed phase column C18 Ultra (5 μm, 4.6× 250 mm) and a spectrophotometric UV detector (SPD-20A). The

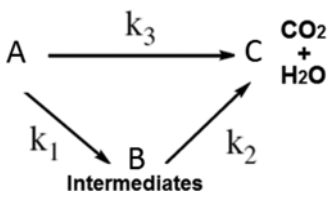

Fig. 1. Reactions to conversion of TOC.

analyses of maximum phenol, resorcinol, catechol and hydroquinone absorption were at 270 nm, while the analyses of p-benzoquinone and of the oxalic, acetic, malonic, maleic, succinic and fumaric acids were at 254 nm. The analyses were under isocratic condition; for the mobile phase separation, a solution of acidified water with phosphoric acid at 10% (v/v) and methanol at a ratio of 90 : 10 was prepared, at a flow rate of 0.750 $mL \cdot min^{-1}$ and pressure of 105 $kgf \cdot cm^{-2}$. The oven temperature was kept at 40±1 °C.

The mineralization used TOC analysis with high-sensitive TOC-VCSH Shimadzu® equipment (4 $\mu gC g^{-1}$-25,000 $mgC g^{-1}$). The TOC was measured by subtracting the inorganic carbon (IC) from the total carbon (TC). The TC was determined by catalytic oxidation of CO_2 after the injection in the sample at 680 °C, while the IC was determined after the reaction of the sample with phosphoric acid (H_3PO_4), 25% (v/v) and its complete conversion to CO_2. The carbon dioxide generated by both processes was measured using non-dispersive infrared detector.

7. Toxicity Tests

Acute toxicity tests were run using seed germination studies. The bioassays were carried out using balsamine (*Impatiens balsamina*), cockscomb (*Celosia cristata*), lettuce (*Lactuca sativa L.*) and wheat (*American hard*) seeds. The seeds were placed in contact with solutions of different concentrations of phenol, before and after the photocatalytic treatment (100%; 70%; 50%; 10%; 5% and 1% (v/v)). A ratio of 10 seeds/grain was added to a 2 mL non-replenished solution of the respective samples for 120 hours; with all trials run threefold, at a temperature of 25±1 °C, in the absence of light. Water was used as negative control, and a solution of boric acid used as a positive control, according to the proposed method [33]. After this period, the number of germinated seeds and the root length were assessed, with the negative control being considered valid when obtaining germination greater than or equal to 90%.

Thus, the root growth index (RGI) and the germination index (GI) were calculated based on the seed germination rates and the root length, according to Eqs. (1) and (2), respectively [34].

$$RGI = \frac{(RS)}{(RC)} \quad (1)$$

$$GI = RGI\frac{(GSS)}{(GSC)} \times 100 \quad (2)$$

where RS is the total root length of the sample, RC is the total root length in the negative control, GSS the number of seeds germinated in the sample and SGC is the number of seeds germinated in the negative control. The measurements were run threefold and the mean and standard deviation calculated (n=3).

RESULTS AND DISCUSSION

1. Catalyst Characterization

Both catalysts used were previously characterized from a structural point of view, based on the following techniques.

1-1. Scanning Electron Microscopy (SEM) with Energy-dispersive X-ray Spectrometry (EDS)

The scanning micrograph of the catalyst ($BiPO_4$) 8000-fold enlarged is presented in Fig. 2(a), in which can be observed that the $BiPO_4$ synthesized by the hydrothermal process was formed by a group of cubic crystals and of irregular sizes, as previously demonstrated. The energy-dispersive x-ray spectrometry graphs (Fig. 2(b)) show that the carbon, oxygen, bismuth and phosphorus are the main elements present in the catalyst, with all EDS spectra gold coated.

Fig. 3(a) shows the scanning micrograph on TiO_2 (P25) 8000-fold enlarged, indicating that TiO_2 was formed by a uniform crystal cluster. In the energy-dispersive X-ray spectrometry (EDS) on commercial TiO_2 (Fig. 3(b)) the presence of carbon, oxygen and titanium can be observed, with similar results being obtained by other authors, who reported the existence of homogeneous crystal clusters (in size and shape) [35,36].

1-2. Fourier Transform Infrared Spectroscopy (FTIR)

In Fig. 4(a), the FTIR spectrum of synthesized $BiPO_4$ is represented by bands at 923.22l; 953.87; 1,007.15 and 1,075.01 cm^{-1}, assigned to the asymmetric stretching vibration of the PO bonds in the PO_4^{3-} group. The bands at 528.07; 553.28; 564.29 and 606.60 cm^{-1} were caused by the asymmetric flexion vibration of the O-P-O bonds in PO_4^{3-}. The bands at 3,441.86 and 16,611.89 cm^{-1} were

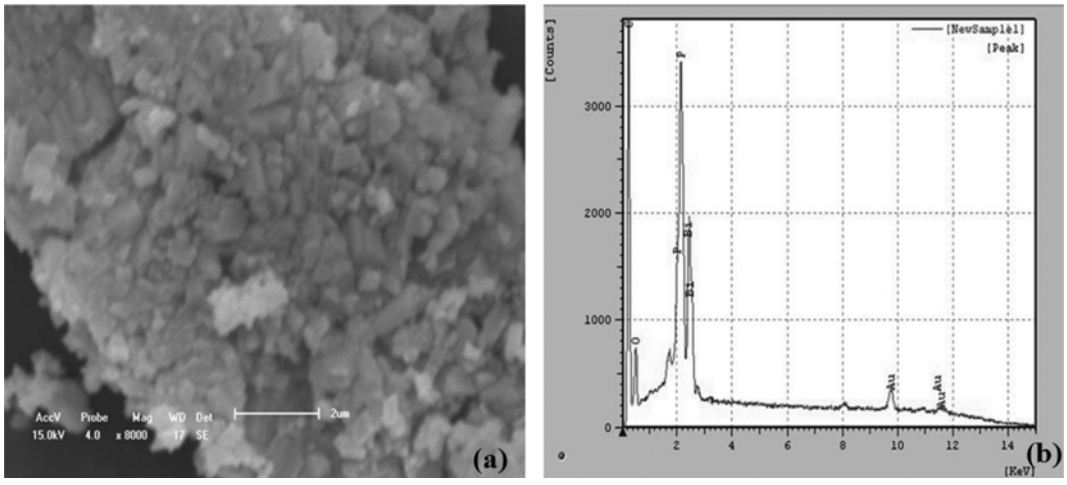

Fig. 2. (a) Micrographs scans for the synthesized $BiPO_4$ with magnification 8,000 times, (b) EDS espectra for the synthesized $BiPO_4$.

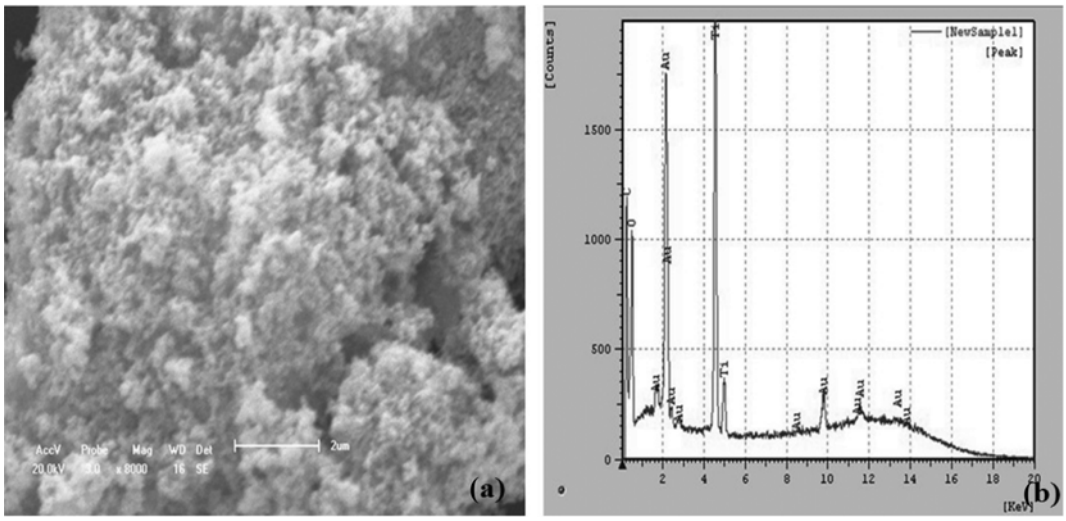

Fig. 3. (a) Micrographs scans for TiO_2 (P25) with magnification 8,000 times, (b) EDS espectra for the TiO_2 (P25).

attributed to the ν(OH) and δ(HOH) bonds, respectively. With the results obtained being very similar to the results presented by other authors for the same composite and caused by the adsorption of water on the catalyst surface [37].

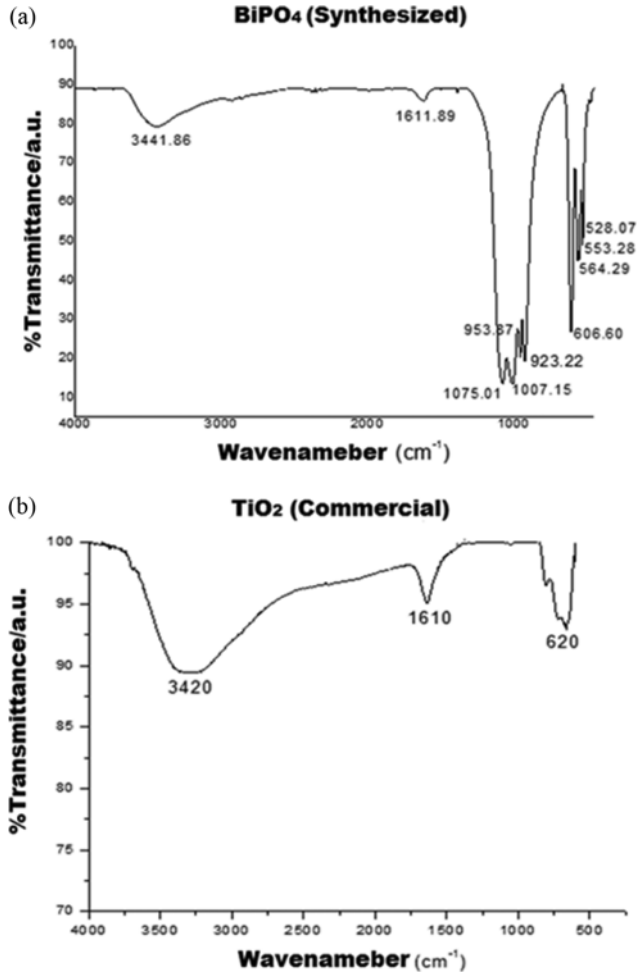

Fig. 4. (a) Infrared spectrum for $BiPO_4$ synthesized by hydrothermal process, (b) infrared spectrum for commercial TiO_2 (P25).

For the TiO_2 particles, the corresponding spectrum IV is shown in Fig. 4(b). The bands at 3,420 and 1,610 cm^{-1} are characteristic of the stretching vibration of the ν(OH) and δ(HOH) bonds, respectively, caused by the adsorbed water over the TiO_2 surface. The typical peak at around 600 cm^{-1} is denoted as the stretching vibration of the Ti-O bond, according to the results for TiO_2, previously stated in the literature [38,39].

1-3. X-ray Powder Diffraction (XRD)

The digital print of the synthesized material was made by x-ray diffraction. Fig. 5(a) shows the powder diffractogram for both catalysts, with the main peaks at 2q=19.03°; 21.34°; 25.21°; 27.16°; 29.10°; 31.26° and 34.52°. Fig. 5(b), the peaks obtained were successfully indexed to the monoclinic crystalline structure of $BiPO_4$, according to the standard norm (JCPDS No.00-015-0767), corroborating with the results described in the biography [40]. With the powder diffractogram of TiO_2 it is possible to identify the characteristic peaks of the crystalline structure, confirming the presence of the anatase phase, according to the standard norm (JCPDS No.00-021-1272), as well as of the rutile phase, according to the standard norm (JCPDS No.01-089-0553). The diffractograms exhibit strong diffraction peaks at 2θ=27°, 36° and 55°, indicating that the TiO_2 was in its rutile phase. The peaks at 2θ=25° and 48° indicate the presence of TiO_2 in the anatase phase. The phase composition, determined by the XRD method, was 81% and 19% for the anatase and rutile phase, respectively, in accordance with the literature [41].

1-4. BET Surface Area Analysis

The catalyst surface area is an important factor which affects the mechanism of the heterogeneous catalysis. Therefore, this parameter was measured to determine the catalytic properties, revealing that both compounds used present a typical mesoporous structure, with surface area of approximately 3.46 and 31.33 m^2g^{-1} for the $BiPO_4$ and TiO_2, respectively.

2. Operational Conditions of Phenol Degradation

2-1. TiO_2/H_2O_2/UV Process

To run the TiO_2/H_2O_2/UV treatment process, a central composite rotational design (CCRD) was applied (Table 1). The concen-

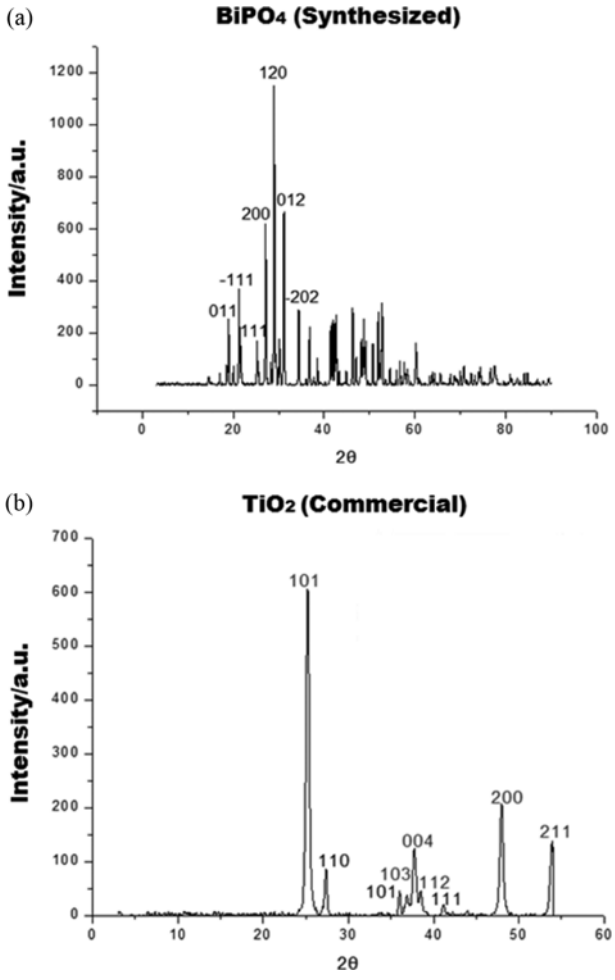

Fig. 5. (a) X-ray diffraction for the synthesized $BiPO_4$, (b) XRD patterns of TiO_2 X-ray (P25).

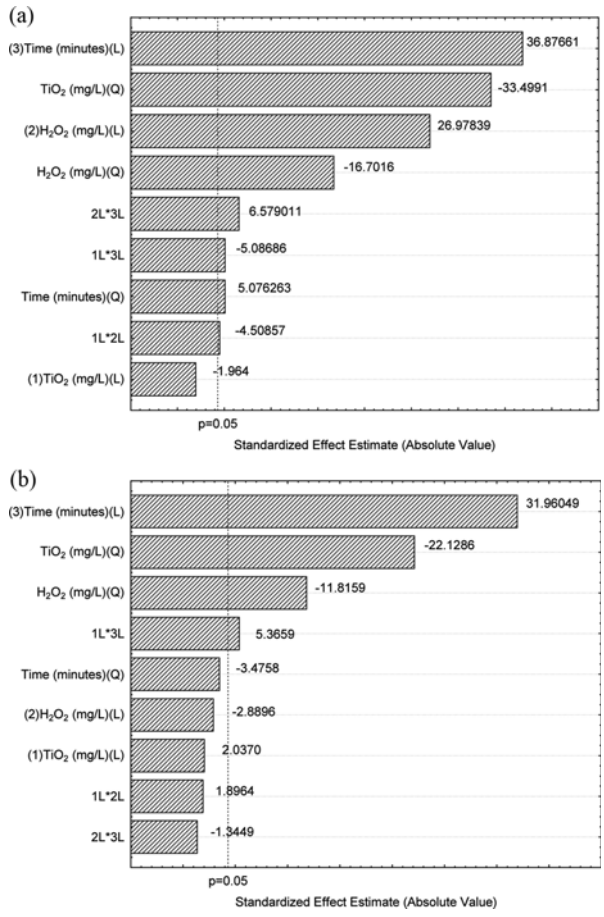

Fig. 6. (a) Effects of all the variables studied for conversion of TOC using TiO_2/H_2O_2/UV process. (b) Effects of all the variables studied for degradation of phenol using the TiO_2/H_2O_2/UV process.

Table 1. Experimental design (CCD) with variables: catalyst (TiO_2 or $BiPO_4$), H_2O_2 and time

Tests	Catalyst (mgL^{-1})	H_2O_2 (mgL^{-1})	Time (minutes)	TiO_2		$BiPO_4$	
				Phenol (%)	TOC (%)	Phenol (%)	TOC (%)
1	−1 (87)	−1 (900)	−1 (120)	85.90	13.30	86.50	30.02
2	1 (174)	−1 (900)	−1 (120)	75.06	10.58	57.60	15.41
3	−1 (87)	1 (1800)	−1 (120)	78.30	23.81	86.54	67.43
4	1 (174)	1 (1800)	−1 (120)	83.98	26.84	67.80	41.44
5	−1 (87)	−1 (900)	1 (240)	85.69	27.10	65.43	43.03
6	1 (174)	−1 (900)	1 (240)	94.16	29.32	59.10	23.70
7	−1 (87)	1 (1800)	1 (240)	92.00	58.89	99.99	95.56
8	1 (174)	1 (1800)	1 (240)	87.00	42.73	96.70	55.16
9	−1.68 (57.34)	0 (1350)	0 (180)	79.90	14.00	98.67	77.00
10	+1.68 (203.66)	0 (1350)	0 (180)	83.45	17.83	71.23	56.00
11	0 (130.50)	−1.68 (593.19)	0 (180)	88.56	21.97	58.50	21.00
12	0 (130.50)	+1.68 (2106.81)	0 (180)	84.67	37.89	95.89	83.39
13	0 (130.50)	0 (1350)	−1.68 (79.09)	81.23	32.80	60.80	20.67
14	0 (130.50)	0 (1350)	+1.68 (280.91)	99.99	63.40	88.23	31.89
15	0 (130.50)	0 (1350)	0 (180)	92.00	43.87	72.00	31.20
16	0 (130.50)	0 (1350)	0 (180)	91.20	42.93	75.60	32.10
17	0 (130.50)	0 (1350)	0 (180)	92.30	41.89	70.90	31.98

trations of H_2O_2 and TiO_2 were used as independent variables over time. The samples were collected from the reactor at different times and, after filtering, stored in an amber flask refrigerator. Figs. 6(a) and 6(b) show the Pareto charts of phenol degradation and mineralization, respectively, enabling the study of the effects of all variables and their interactions. The y-axis represents the independent variable or the interaction between the variables, while the x-axis represents the absolute value of the effects calculated as the ratio between the effects and their standard-deviation. The effects were considered significant at a confidence level of 95%, which corresponds to the bars beyond the p=0.05 line.

Fig. 6(a) illustrates the effects of the variables H_2O_2, TiO_2 and time, respectively. From the results it can be observed that the reaction time is the most-influential variable in the process. With this same diagram, it can also be verified the relevance of all interactions involved in the process, except for the main linear effect of the concentration of TiO_2.

Time is considered the most significant variable, with strongest influence on both parameters in the linear response function. However, the quadratic response function is of strongest influence on the results for TiO_2 and H_2O_2 (Fig. 6(b)). It is possible to preview the optimized parameters when using the response surface method, using a 3D graph, as shown in Figs. 7(a) to 7(c).

As seen in Fig. 7(a), there was a marked increase in the amount of TOC converted over the reaction time and the amount of H_2O_2. Increasing the reaction time guarantees a better product formation, and consequently the rupture of the molecules of the most efficient composite. Fig. 7(b) demonstrates the relation of the TiO_2 interaction with the reaction time between 240 and 300 minutes, for concentrations ranging from 70 to 170 mgL^{-1}.

The amounts of TOC obtained show a higher conversion for TiO_2 concentrations varying between 80 and 180 mgL^{-1}. According to the statistical analysis, the TOC conversion process is most efficient for H_2O_2 and TiO_2 concentrations of 1,350 and 130.50 mgL^{-1}, respectively; which corroborates the previous data obtained for the response surfaces (see Fig. 7(c)). Selecting the optimal catalyst concentration is essential, to minimize its surplus, ensuring the complete absorption of photons. As seen in Fig. 8, the increase of TOC conversion on the catalyst concentration is extended up until approximately 130.50 mgL^{-1}. Whenever the catalyst concentration rises, the phenol degradation level decreases due to the shielding effect caused by the surplus particles that mask the photosensitive surface, therefore affecting the light penetration.

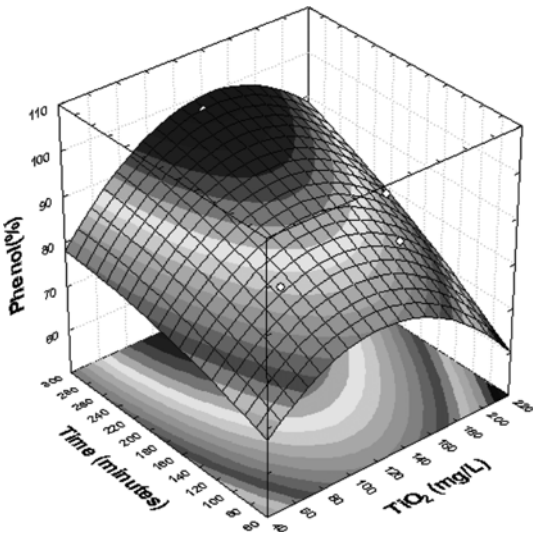

Fig. 8. Response surfaces for the degradation of phenol with time (mintutes) vs. TiO_2 concentration (mgL^{-1}).

2-2. $BiPO_4/H_2O_2$/UV Process

To run the $BiPO_4/H_2O_2$/UV process, a central composite rotational design (CCRD) was used (Table 1), with H_2O_2 and $BiPO_4$ concentrations and time (minutes) as independent variables. The same procedure described in the previous treatment was used to collect and store the samples studied. Table 1 shows the results obtained for the percentage of phenol degradation and TOC conversion values.

As previously mentioned, catalyst conversion is an important parameter in photocatalysis in order to guarantee an efficient degradation of phenol. According to Table 1 and to the comparison tests 1 to 8, both the phenol degradation and mineralization (TOC) decrease as the amount of catalyst increases. This is due to the aggregation and sedimentation of the catalyst particles, resulting in

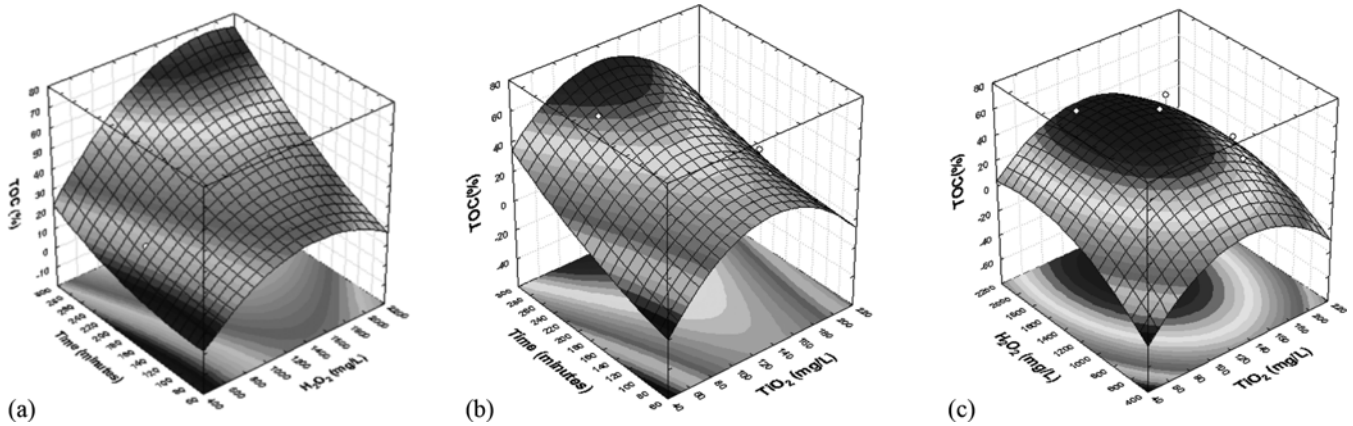

Fig. 7. Response surfaces for TOC mineralization. (a) Time (minutes) vs H_2O_2 ($mg{\cdot}L^{-1}$); (b) =time (minutes) vs TiO_2 ($mg{\cdot}L^{-1}$); (c) =H_2O_2 ($mg{\cdot}L^{-1}$) vs TiO_2 ($mg{\cdot}L^{-1}$).

a smaller interfacial area catalyst/phenol, and also due to the increase in turbidity in the sample, therefore affecting the penetration and dispersion of light [42]. Tests 9-17, including the central axial points, demonstrated that the degradation of phenol was unsuccessful when compared to other experiments. Besides the values provided by test 9, all other tests affirmed that the efficiency of the degradation of phenol is related to the increase of the amount of catalyst.

As seen, the increase of peroxide concentration has a positive effect in the degradation and mineralization of phenol, though an excess in concentration may cause side effects (trial 12). Analyzing the variable time establishes that the increase of concentration also boosts the efficiency of the degradation of phenol up until a certain amount (trial 14). For the $BiPO_4$ and under the conditions studied, the best results were of 99.99% and of 95.56% for the degradation and mineralization of phenol, respectively; with a reaction time of 240 min for 87 mgL^{-1} of $BiPO_4$ and 1,800 mgL^{-1} of H_2O_2. In these experimental conditions, the percentage of TOC conversion in the $BiPO_4/H_2O_2$/UV process (around 40%) was higher than for the TiO_2/H_2O_2/UV process. Figs. 9(a) and 9(b) show the influence of the variables in the photocatalytic process, using Pareto charts to describe the degradation of phenol and the TOC conversion, respectively.

The effects of the interaction between the variables time and the concentrations of H_2O_2 and $BiPO_4$ were accounted as being statistically significant to the confidence level of 95% (Fig. 9(a)). However, the interaction between $BiPO_4$ and H_2O_2 was not considered statistically significant in terms of the degradation of phenol; though, when analyzing Fig. 9(b) in respect to the TOC conversion, the interaction of all variables and their interactions was statistically significant. Figs. 10(a), 10(b) and 10(c) show the contour plots of the response surfaces for the TOC as a function of H_2O_2 and $BiPO_4$, indicating the propensity of the process.

The highest TOC degradation trends were reached decreasing the amount of catalyst and increasing both the reaction time and the concentration of H_2O_2. For lower concentrations of both the catalyst $BiPO_4$ and of H_2O_2 in the blue area, an inferior level of TOC was obtained. The opposite is observed in the red area; above the central points there are higher mineralization levels when the concentration of $BiPO_4$ is low and the concentration of H_2O_2 is high. The efficient mineralization increases over time (Fig. 7(b) and 7(c)); Figs. 11(a) and 11(b) show the response surfaces and the curve

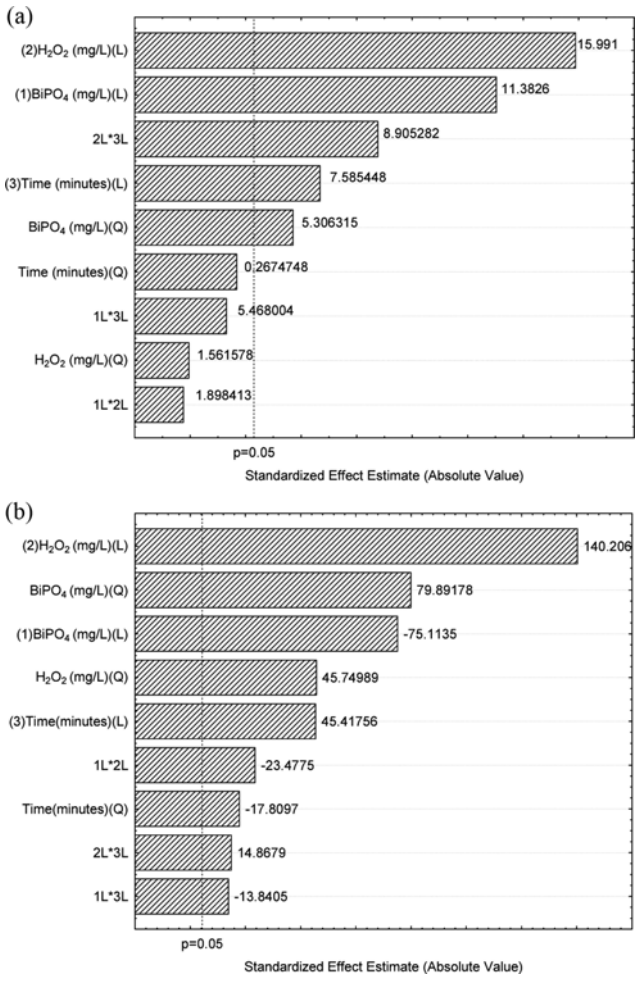

Fig. 9. (a) Effects of all the variables studied for degradation of phenol using the $BiPO_4/H_2O_2$/UV process. (b) Effects of all the variables studied for conversion of TOC using the $BiPO_4/H_2O_2$/UV process.

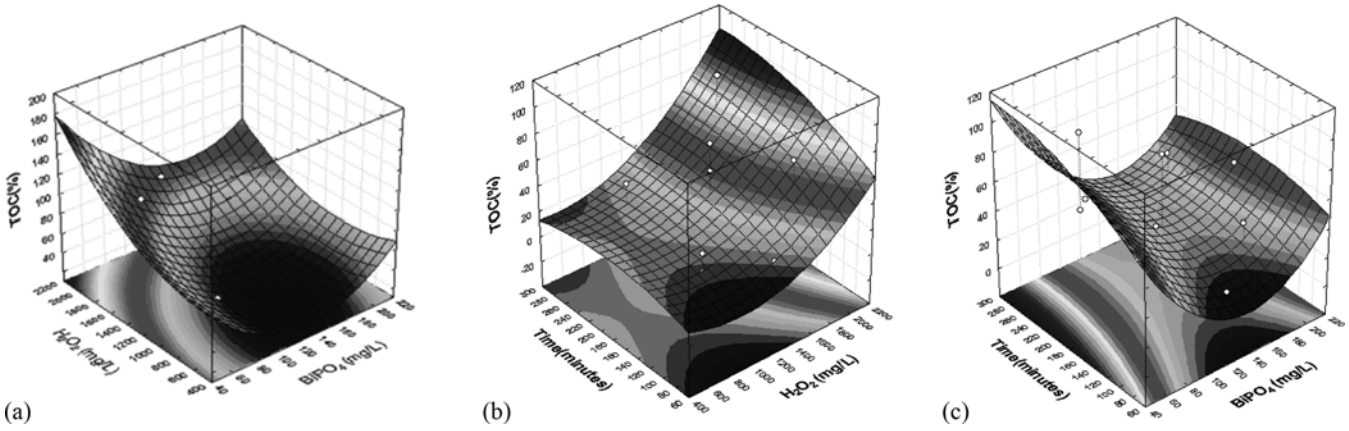

Fig. 10. Response surfaces for TOC mineralization. (a) =$BiPO_4$ ($mg{\cdot}L^{-1}$) vs H_2O_2 ($mg{\cdot}L^{-1}$); (b) =H_2O_2 (mmol) vs time (minutes); (c) =time (minutes) vs $BiPO_4$ ($mg{\cdot}L^{-1}$).

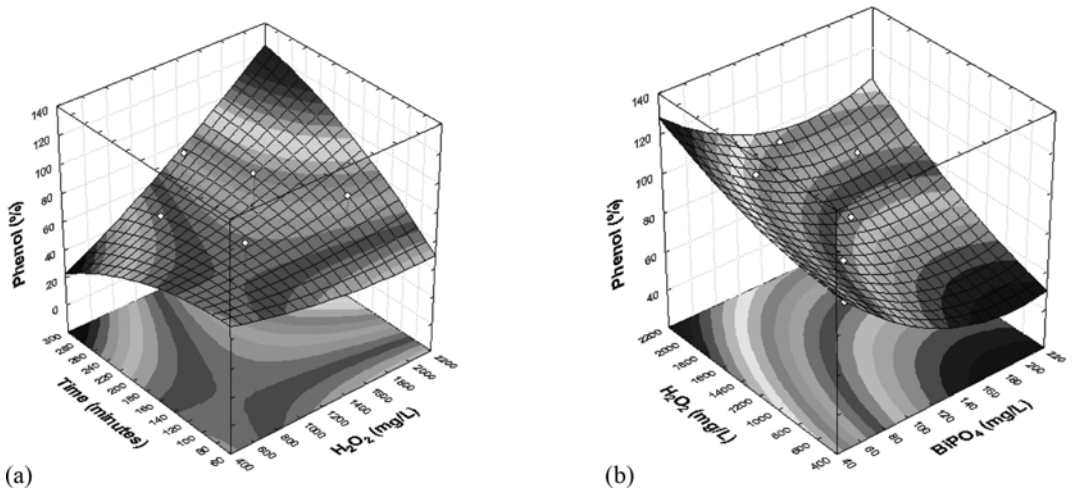

Fig. 11. Response surfaces for phenol degradation. (a) =time (mintutes) vs H_2O_2 ($mg \cdot L^{-1}$); b) =H_2O_2 (mmol) vs $BiPO_4$ ($mg \cdot L^{-1}$).

fitting with the quadratic model when the degradation of phenol is carried out using the $BiPO_4/H_2O_2$/UV process. The degradation could be, however, improved if the concentration of $BiPO_4$ was fixed to a maximum value of 60 mgL^{-1} (Fig. 11(a)); with the reaction time being of 120 minutes under these conditions, and the degradation of phenol increasing significantly with a rise in H_2O_2 concentration and reaction time (Fig. 11(b)).

Fig. 12(a) represents the intermediate formed, detected during the reaction of degradation of phenol using the $BiPO_4/H_2O_2$/UV process under the following conditions: 87 mgL^{-1}, 1,800 mgL^{-1} in 240 minutes at a pH=4.

The sub-products obtained were hydroquinone, resorcinol, p-benzoquinone and malonic, maleic, fumaric and acetic acids. The evolution of the organic acids indicates the progression of the reaction, as they are initially for oxidizing the CO_2 [43]. Authors such as Liu et al. [29] analyzed the degradation of phenol, using the same catalyst at a pH=5.8, with 4.4-dihydroxibiphenil as a primary intermediate; other compounds such as hydroquinone, p-benzoquinone and catechol and carboxylic acids were not detected.

The presence of organic acids in 120 minutes indicates that the time was not enough to complete the mineralization; a reaction time of 240 minutes corresponds to an almost complete degradation of phenol. Under the conditions studied no other additional treatment was required, as 95.56% of TOC was converted in CO_2 and water. This value is within the boundaries established by the norms proposed by the CONAMA 437/2011, Brazil.

For the TiO_2/H_2O_2/UV process, represented in Fig. 12(b), the following conditions were determined for the intermediate compounds formed: 130.50 mgL^{-1} of TiO_2, 1,800 mgL^{-1} of H_2O_2, with pH=6, at a reaction time of 281 minutes. Comparing the results obtained for the $BiPO_4$ catalyst and the reaction time of 240 minutes (Fig. 12(b)), a significant presence of organic acids, including the maleic acid, could be observed, with similar sub-products being found by other authors [44], demonstrating the tendency of the

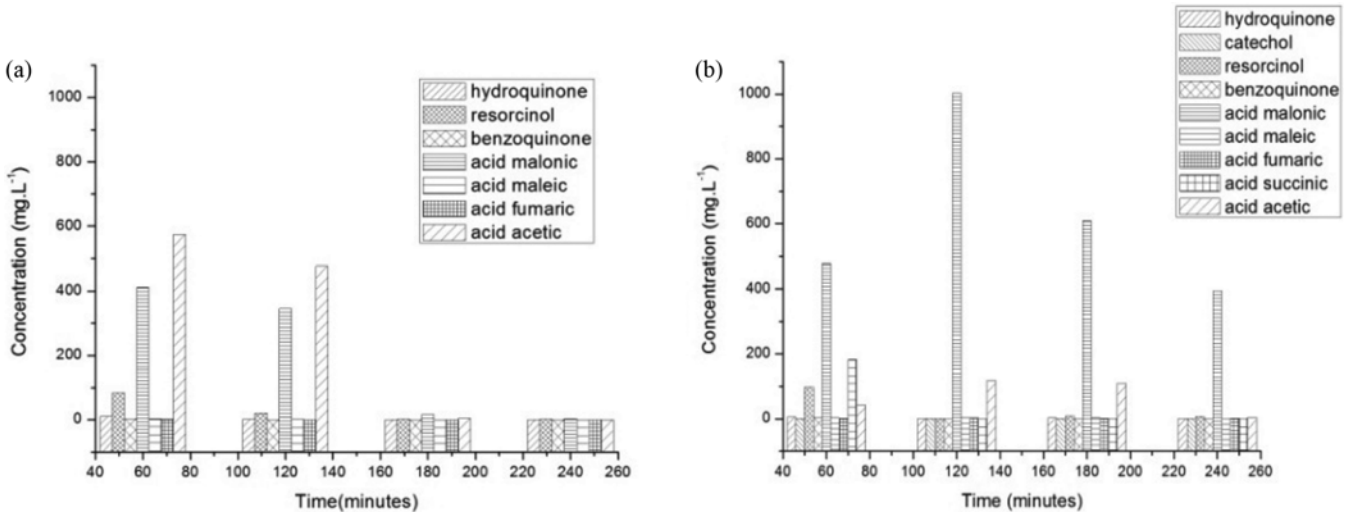

Fig. 12. (a) Phenol intermediates observed applying $BiPO_4/H_2O_2$/UV treatment; (b) phenol intermediates observed applying TiO_2/H_2O_2/UV treatment.

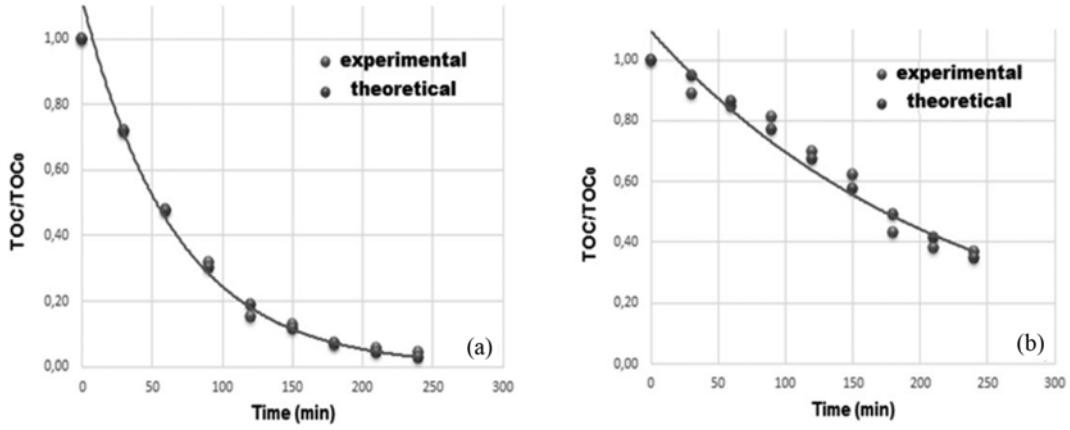

Fig. 13. (a) Model set kinetic grouped to the experimental data conversion TOC by $BiPO_4$/ H_2O_2/UV process in its optimum operating condition: [$BiPO_4$]=87 mg·L^{-1}. [H_2O_2]=1,800 mg·L^{-1}. pH=4. T=25 °C; (b) model set kinetic grouped to the experimental data of the TOC conversion process by TiO_2/H_2O_2/UV in its optimum operating condition: [TiO_2]=87 mg·L^{-1}. [H_2O_2]=1,800 mg·L^{-1}. pH=6. T=25 °C.

products forming catechol and hydroquinone. According to [45], compounds such as hydroquinone, catechol and p-benzoquinone were also identified.

3. Kinetic Study

The evolution of the TOC mineralization is graphically represented (Fig. 13(a)) as a function of time after the $BiPO_4/H_2O_2$/UV treatment process. The values of the constants k were estimated by linear regression, those being of 0.036 min^{-1}, 0.016 min^{-1} and 0.008 min^{-1} for k_1, k_2 and k_3, respectively, and with R^2=0.9977. As it can be observed, k_1 two-fold than the reaction k_2 (phenol/intermediate) is about three times faster than the intermediates in the reaction/ CO_2+H_2O. The phenol/CO_2+H_2O with k_3=0.008 min^{-1} is however much slower in comparison with the other reactions involved. According to [46], the k_1 value for the correspondent phenol transformation into intermediate compounds is, in most cases, more elevated, followed by k_2, related to the intermediate products of the final substrates, characteristic of oxidative processes, according to the same author.

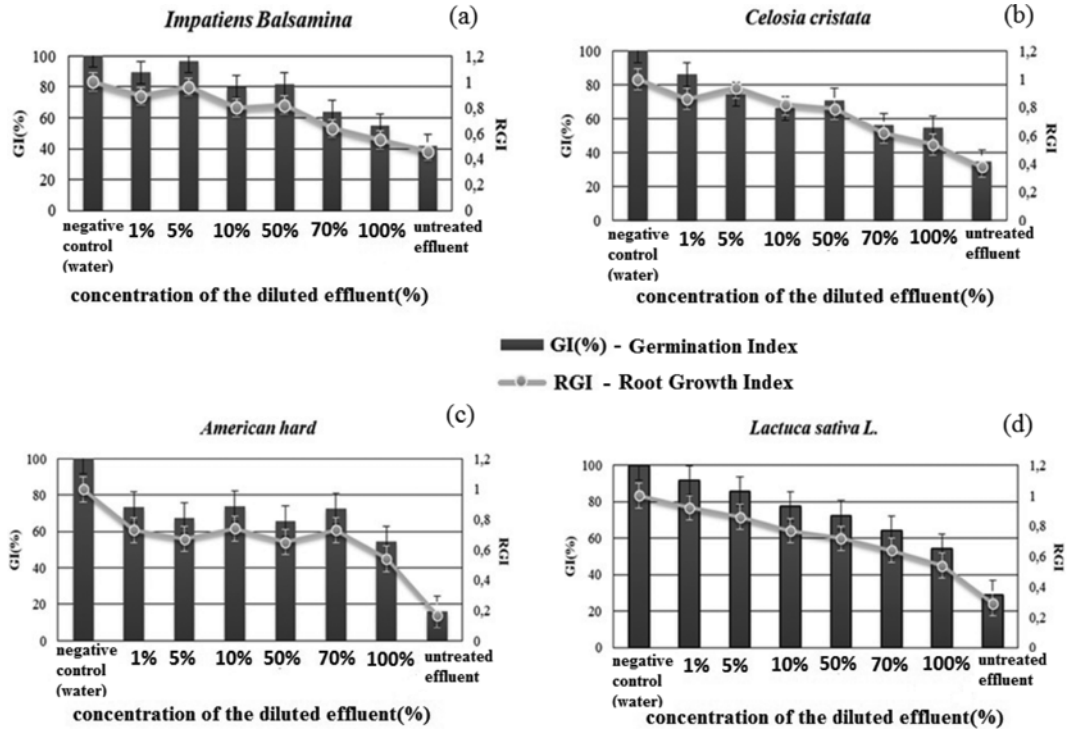

Fig. 14. Root growth index of (RGI) and the germination index (GI) of seeds (a) *Impatiens balsamina*, (b) *Celosia cristata*, (c) *American hard* and (d) *Lactuca sativa* as a function of effluent concentration: 100%, 70%, 50%, 5% and 1%, and before being subjected to $BiPO_4$/ H_2O_2/UV treatment.

For the TiO_2/H_2O_2/UV system, the values for the constants k_1, k_2 and k_3 were of: 0.08 min^{-1}, 0.09 min^{-1} and 0.001 min^{-1}, respectively, with R^2=0.9701; noting that k_1 was almost equal to k_2, meaning that the reaction with phenol/intermediates and the intermediate compounds/CO_2+H_2O were formed in the same intensity. Note that the constant k_3 (k_3=0.001 min^{-1}) was lower than k_1 and k_2, showing no direct degradation of phenol in CO_2+H_2O.

4. Toxicity

The toxicity tests are fundamental analyses carried out to guarantee the quality of the material to be disposed. It is therefore essential to find reliable pollution indicators, with enough sensitivity for light environmental changes. The eco-toxicological trials are relatively simple, easy to handle and do not require a sophisticated environment for their development. The toxicity tests involved using different types of seeds and also evaluating the degree of germination, when placed in contact with the phenol samples before and after being treated by the advanced oxidation processes. The trials were run with solutions at different concentrations of phenol after being treated by the $BiPO_4/H_2O_2$/UV and TiO_2/H_2O_2/UV processes. The results obtained were expressed in terms of the total root growth of each seed, based on the Root Growth Index (RGI) and the Germination Index (GI (%)).

The graphs represented in Figs. 14(a) to 14(d) show the results for the GI (%) and the RGI corresponding to the germination of the several seed types at different phenol dilutions (1 to 100%) after being treated using the $BiPO_4/H_2O_2$/UV process. The results for the germinations studied in non-treated solutions were also represented for comparison purposes.

Although the species survived, their growth was considered limited, due to the toxic conditions for lethal (inhibition of germination) and sub-lethal (inhibition of root development) effects, caused by the toxic pollutants [34].

The percentages of inhibition of germination were 60% for the balsamine seed, 70% for cockscomb, 80% for wheat and 70% for lettuce, respectively, demonstrating the high toxicity of phenol in these types of organisms.

As for the root growth, and for the same dilution level, the inhibition of germination for the treated solution was approximately 15%, 40%, 60% and 30% for balsamine, cockscomb, wheat and lettuce, respectively, therefore concluding that the photocatalysis treatment contributes in reducing the acute toxicity in the different types of seeds. Although during the oxidation process intermediates compounds are formed because of the treatment process applied, these are considered less toxic than the main compound. Similar results were also published by Brito-Pellegrini et al. [47], where a reduction of about 80% in toxicity was observed for wastewater treated using AOP processes (homogeneous and/or heterogeneous).

The degradation processes using the TiO_2/H_2O_2/UV system are presented in Figs. 15(a) to 15(d); being observed an increase of 23.63, 4.11 and 6.75% of the GI (%) for balsamine, cockscomb and wheat, respectively. Regarding lettuce, a reduction of approximately 4.33% in germination could be observed, before and after the treatment; with a possible link to the intermediate products formed during the degradation process when using the TiO_2/H_2O_2/UV process.

Similar results were reported by Rizzo et al. [48] and Clément et al. [49], reinforcing the importance of studying not only the toxic-

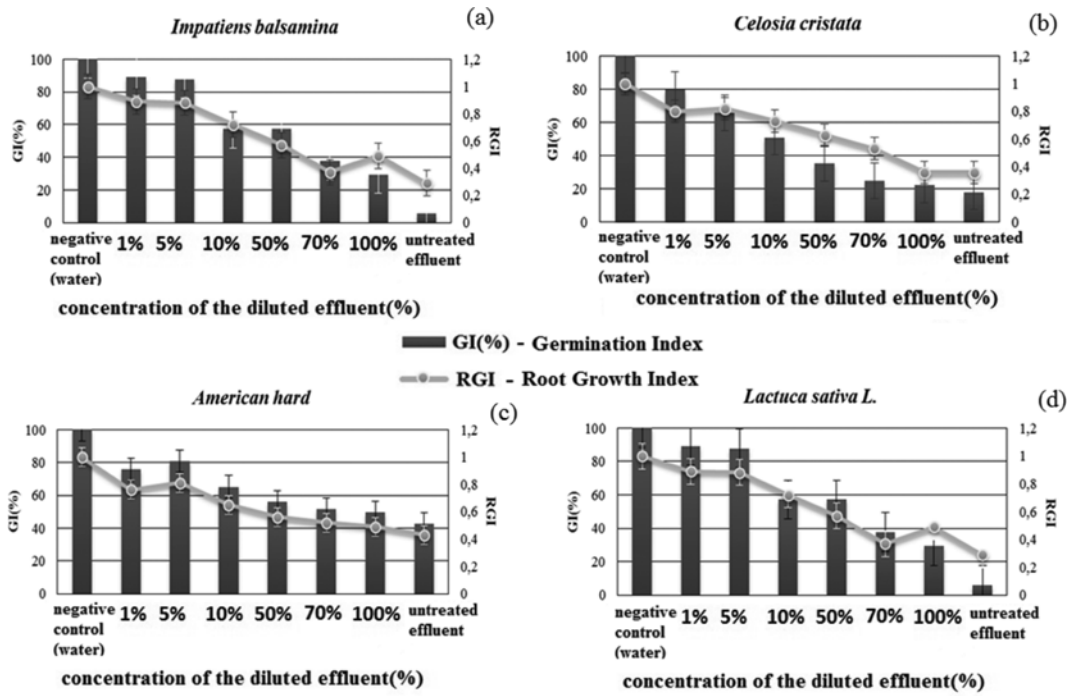

Fig. 15. Root growth index of (RGI) and the germination index (GI) of seeds (a) *Impatiens balsamina*, (b) *Celosia cristata*, (c) *American hard* and (d) *Lactuca sativa* as a function of effluent concentration: 100%, 70%, 50%, 5% and 1%, and before being subjected to TiO_2/H_2O_2/UV treatment.

ity of effluents before and after the treatment process, but also exploring the catalysts used in the toxicity studies applied to the treatment of wastewater.

This result was important because of the link between this parameter and the eco-toxicological trials, usually with substantial reductions in organic matter in such a complex matrix like phenol. The eco-toxicological trials were fundamental to guarantee the quality of the material to be disposed; finding sensitive organisms that respond to the chemical alteration in the environment is important to guarantee an efficient eco-toxicological trial.

CONCLUSION

Two types of heterogeneous oxidation processes were used, and submitted to the TiO_2/H_2O_2/UV and $BiPO_4/H_2O_2$/UV processes for the degradation and mineralization of phenol; with statistical models being applied to asses which were the most relevant variables in the process. The results showed that although phenol was rapidly removed, the mineralization was not completed when using the TiO_2/H_2O_2/UV system; having obtained 99.99% and 63.40% for the removal and mineralization of phenol, respectively, under the following optimised conditions: $[TiO_2]$=130.50 mg·L^{-1}, $[H_2O_2]$= 1.350 mg·L^{-1}, time=281 minutes. The $BiPO_4/H_2O_2$/UV process was revealed as being the most efficient process, having obtained 99.99 and 95.56%, under $[BiPO_4]$=87 mg·L^{-1}, $[H_2O_2]$=1,800 mg·L^{-1}, time= 240 minutes. In this case, although the characterization studies showed a smaller surface area for the $BiPO_4$ in relation to TiO_2, higher levels of mineralization of phenol were obtained. Both kinetic studies revealed that the degradation of phenol occurred with the production of intermediate compounds. The acute toxicity tests applied to the oxidation treatments demonstrated better results when using the $BiPO_4/H_2O_2$/UV process; with its use being therefore supported in the treatment of wastewater.

ACKNOWLEDGEMENTS

The authors would like to express their upmost gratitude to FACEPE/NUQAAPE. CAPES. CNPQ/INCTAA for financial support.

REFERENCES

1. J. B. Mariano, *Impactos ambientais do refino de petróleo*, Tese (Mestrado em Ciências em Planejamento Energético) - UFRJ. Rio de Janeiro (2001).
2. J. M. Brito and M. C. Rangel, *Química Nova. São Paulo.*, **31**(1), 114 (2008).
3. M. Asghari and M. A. Rakhshanikia, *Procedia - Social and Behavioral Sciences*, **75**, 264 (2013).
4. A. Coelho, *J. Hazard. Mater.*, **137**(1), 178 (2006).
5. O. Abdelwahab, N. K. Amin and E. S. Z. El-ashtoukhy, *J. Hazard. Mater.*, **163**, 711 (2009).
6. J. García-pérez, V. Lope, G. López-Abente, M. González-Sánchez and P. Fernández-Navarro, *Environ. Pollution*, **205**, 103 (2015).
7. S. K. Pardeshi and A. B. Patil, *Solar Energy*, **82**(8), 700 (2008).
8. M. H. El-Naas, S. Al-Zuhair and M. A. Alhaija, *J. Hazard. Mater.*, 750 (2009).
9. O. Osibanjo, A. P. Daso and A. M. Gbadebo, *African J. Biotechnol.*, **10**, 696 (2011).
10. W. Zhong, D. Wang and X. Xu, *J. Hazard. Mater.*, **217-218**, 286 (2012).
11. S. Yang, W. Zhu, J. Wang and Z. Chen, *J. Hazard. Mater.*, 1248 (2008).
12. J. Moreira Del Rio, *Photocatalytic degradation of phenolic compounds in water: Irradiation and kinetic modeling. tese de doutorado*, University of Western Ontario, London, Ontario, Canada (2011).
13. W. Zhong, D. Wang and X. Xu, *Chinese Academy of Sci.*, **217-218**, 286 (2012).
14. Y. Yavuz and A. S. Koparal, *J. Hazard. Mater.*, **136**(2), 296 (2006).
15. C. E. Santo, J. P. Vilar, C. M. S. Botelho, A. Bhatnagar, E. Kumar and R. A. R. Boaventura, *Chem. Eng. J.*, **183**, 117 (2012).
16. J. Saien and H. Nejati, *J. Hazard. Mater.*, **148**(1-2), 491 (2007).
17. K. Tong, Y. Zhang, G. Liu, Z. Ye and P. K. Chu, *International Biodeterioration Biodegradation*, **84**, 65 (2013).
18. Y. Huang, Y. Huang, H. Tsai and H. Chen, *J. Taiwan Ins. Chem. Engineers.*, **41**, 699 (2010).
19. A. Karci, I. Arslan-Alaton, T. Olmes-Hanci and M. Bekbolet, *J. Photochem. Photobiol. A: Chem.*, **230**, 65 (2012).
20. T. Olmez-Hanci and I. Arslan-Alaton, *Chem. Eng. J.*, **224**, 10 (2013).
21. N. Merayo, D. Hermosilla, L. Blanco, L. Cortijo and A. Blanco, *J. Hazard. Mater.*, 420 (2013).
22. M. Mehrjouei, S. Muller and D. Moller, *J. Environ. Manage.*, **120**, 68 (2013).
23. D. Avisar, I. Horovitz, L. Lozzi, F. Ruggieri, M. Baker, M. L. Abel and H. Mamane, *J. Hazard. Mater.*, **244-245**, 463 (2013).
24. N. A. M. Barakat, M. A. Kanjwal, I. S. Chronakis and H. Y. Kima, *J. Mol. Catal. A: Chem.*, **366**, 333 (2013).
25. E. Rego, J. Marto, P. São Marcos and J. A. Labrincha, *Appl. Catal. A: Gen.*, **355**, 109 (2009).
26. M. P. Seabra, E. Rego, A. Ribeiro and J. A. Labrincha, *Chem. Eng. J.*, **171**, 175 (2011).
27. Y. Zhang, Q. Xin, Y. Cong, Q. Wang and B. Jiang, *Chem. Eng. J.*, **215-216**, 261 (2013).
28. J. M. Bothwell, W. Scott, W. Krabbez and R. S. Mohan, *Chem. Soc. Rev.*, **40**, 4649 (2011).
29. Y. Liu, Y. Zhu, X. Bai, R. Zong and Y. Zhu, *Appl. Catal. B: Environ.*, **142-143**, 562 (2013).
30. J. Xu, L. Li, C. Guo, Y. Zhang and W. Meng, *Appl. Catal. B: Environ.*, **130-131**, 285 (2013).
31. L. Pan, X. Liu, Z. Sun and C. Sun, *J. Mater. Chem. A.*, **1**, 8299 (2013).
32. Q. Zhang and K. T. Chuang, *AIChE J.*, **45**(1), 145 (1999).
33. American society for testing and materials - astm, Standard Guide for Condunting Terrestrial Plant Toxicity Tests, E 1963 - 02 (2002).
34. S. M. Palácio, D. A. Nogueira, D. R. Manenti, A. N. Módenes, F. R. E. Quiñones and F. H. Borba, *Engevista.*, **14**, 127 (2012).
35. B. Long, J. Huang and X. Wang, *Mater. Int.*, **22**, 644 (2012).
36. S. Wu, H. Zheng, Y. Lian and Y. Wu, *Mater. Res. Bulletin.*, **48**, 2901 (2013).
37. Z. Zhao, Y. Zhou, W. Wan, F. Wang, Q. Zhang and Y. Lin, *Mater. Lett.*, **130**, 150 (2014).
38. D. Bem Luiz, S. L. F. Andersen, C. Berger, H. J. José and R. F. P. M.

Moreira, *J. Photochem. Photobiol. A: Chem*., **246**, 36 (2012).
39. F. Xue, H. Li, Y. Zhu, S. Xiang, T. Wang, X. Liang and Y. Qian, *J. Solid State Chem*., **182**, 1396 (2009).
40. E. Kabachko and E. Kurkin, *J. Photochem. Photobiol. A: Chem*., **217**, 425 (2011).
41. Z. He, W. Que, J. Chen, Y. He and G. Wang, *J. Phys. Chem. Solids*, **74**, 924 (2013).
42. D. N. Clausen and K. Takashima, *Química Nova*, **30**(8), 1896 (2007).
43. J. A. Zazo, J. A. Casas, A. F. Mohedano and J. J. Rodriguez, *Water Res*., **43**, 4063 (2009).
44. M. Bellardita, V. Augugliaro, V. Loddo, B. Megna, G. Palmisano, L. Palmisano and M. A. Puma, *Appl. Catal. A: Gen*., **441-442**, 79 (2012).
45. D. Zhang, R. Qiu, L. Song, B. Eric, Y. Mo and X. Huang, *J. Hazard. Mater*., **163**, 843 (2009).
46. E. B. Azevedo, A. R. Tôrres, F. R. Aquino Neto and M. Dezotti, *Brazilian J. Chem. Eng*., **26**, 75 (2009).
47. N. N. Brito-Pelegrini, J. E. S. Paterniani, G. A. Brota, E. M. Santos, N. B. Silva and R. T. Pelegrini, *Minerva*, **6**, 219 (2009).
48. L. Rizzo, S. Meric, M. Guida and D. Kassinos, *Water Res*., **43**, 4070 (2009).
49. L. Clément, C. Hurel and N. Marmier, *Chemosphere*, **90**, 1083 (2013).